Spectroscopic characterization of CuOx/TiO2–ZrO2 catalysts prepared by a-step sol–gel method

Spectroscopy characterization of CuO_x/TiO_2-ZrO_2 catalysts prepared by one step sol-gel method

F. Morales Anzures,[1] F. Chávez Rivas,[2,§,*] J. Hernández Ventura,[1] P. Salinas Hernández,[1] G. Berlier[2*] and G. Zacahua-Tlacuatl[3]

[1] Universidad del Istmo, Campus Tehuantepec, Instituto de Estudios de la Energía, Tehuantepec, Oaxaca, México; fmanzures@yahoo.com.mx

[2] Università di Torino, Dipartimento di Chimica and NIS Centre, Via P. Giuria 7, 10125 Torino, Italy.

[3] Laboratorio de Posgrado, ESIQIE-IPN, UPALM., C. P. 07738. México D.F., México.

Abstract

Copper-titania-zirconia mixed oxides with TiO_2/ZrO_2 1:1 atomic ratio and copper content of 1, 3 and 5 wt % were prepared by one step sol-gel method. X Ray Diffraction and gas-volumetric analysis showed poor crystallinity and high specific surface area (around 250 m^2/g) of the catalysts calcined at 400 °C. The nature of the copper species in the mixed oxides was characterized by Temperature Programmed Reduction in hydrogen (TPR), low temperature Electron Paramagnetic Resonance (EPR) and Diffuse Reflectance (DR) UV-Vis spectroscopies. These techniques suggested the presence of different copper species including distorted octahedral Cu^{2+} ions (isolated or quasi-isolated) in the solid solution bulk, characterized by a TPR peak above 400 °C (labeled as T1), electronic d-d transitions around 800 nm and an anisotropic EPR signal with two hyperfine interactions in the g|| region. The symmetry of this site changed from rhombic (S1) to axial (S3) while increasing copper loading. The inclusion of copper ions in the TiO_2-ZrO_2 matrix was also testified by changes in the mixed-oxide edge position. Two families of supported copper oxide were found. CuO "bulk-like" showed relatively high reduction temperature (T2, around 250 °C), while highly dispersed CuO_x nanoparticles/clusters resulted in TPR peaks around 170 and 200 °C (T4 and T3). These species were responsible for the UV-Vis adsorption above 400 nm and for the broad and asymmetric axial EPR signal with g|| in the range from 2.14 to 2.29 (S2 and S2'). Finally, 2-propanol decomposition was employed as a test reaction to probe surface acid/base character. The results suggested a marked effect of copper loading on the reactivity pattern, confirming the presence of CuO/CuOx particles on the surface of the TiO_2-ZrO_2 support.

Keywords: titania-zirconia; copper oxide; XRD; TPR; DR UV-Vis; EPR

[§]On leave from ESFM-IPN-Mexico. *Corresponding authors: fchavez@esfm.ipn.mx and gloria.berlier@unito.it

1. Introduction

Copper is an important element in catalysis, due to the redox properties which can be exploited in many catalytic processes. For instance, Cu-zeolites have been extensively studied for Selective Catalytic Reactions of NOx (SCR) reactions [1, 2] and are still the subject of attention in this field particularly for NH3-SCR [3-5]. In these catalysts copper is usually present as counterion in the 2+ or +1 oxidation state depending on the thermal activation and preparation conditions [5, 6]. Other important applications of copper in catalysis are related to CuO supported on different oxides. These ranges from CuO on ZnO, Al_2O_3, MgO, for dehydrogenation of cyclohexanol to cyclohexanone and aromatization of cyclohexanol to phenol [7], to CO oxidation on CuO/CeO_2 and $CuO/ZrCeO_4$ catalysts and Cu/Mn co-loaded mesoporous ZrO_2-TiO_2 [8, 9]. Cu/SiO_2 catalysts were instead reported for ester hydrogenolysis reactions [10]. The nature of active copper sites in this kind of catalysts has not been deeply studied in the literature.

Among oxidic supports, TiO_2-ZrO_2 mixed oxide has been widely employed for various applications due to its acidic properties and good mechanical properties [11, 12]. It has been reported as support for metallic nanoparticles, such as Pt for CO oxidation in diesel exhaust devices [13] or gold nanoparticles on CeO_2/TiO_2-ZrO_2 for CO removal by low temperature water–gas shift reaction [14]. The same support was employed in the NO reduction by propene with both Ag or In as active species [15, 16]. Supported metal oxides were also reported. For instance tungsten oxide loaded on TiO_2-ZrO_2 was found to have a high activity into the decomposition of chlorofluorocarbons in the presence of water vapor [17].

Most of the above mentioned catalysts based on metals and metal oxides supported on the TiO_2-ZrO_2 matrix are usually synthesized in two steps. These involves the synthesis of the mixed oxide support and the following deposition of the surface active species by impregnation, incipient wetness or wet precipitation. An excellent review up to 2005 of the mentioned methods in the synthesis of metals and oxide metals supported on TiO_2-ZrO_2 matrices can be find in Ref. [18]. TiO_2-ZrO_2 is usually prepared by solid state reactions, mixing titanium oxide and zirconium oxide at temperatures above 1400 °C [19], however, this method produces materials with very small specific surface area (SSA). On the contrary, samples prepared by sol-gel method were reported to show high SSA at low synthesis temperature [20]. By this approach it is possible to control hydrolysis rate and condensation of the molecular precursors used [21, 22]. When preparing mixed oxides, the difference in reactivity of the two precursors can be minimized by controlling the pre-hydrolysis of the less reactive one or by their chemical modification.

The objective of this work is to study the effect of the copper loading in mixed TiO_2-ZrO_2 oxides prepared by the sol-gel method and calcined at 400 °C. The catalysts were characterized by X-ray diffraction (XRD), gas-volumetric analysis, temperature programmed reduction (TPR), diffuse reflectance in the ultraviolet-visible range (DR UV-Vis) and electron paramagnetic resonance (EPR) spectroscopies. The catalytic activity of the materials in the decomposition of isopropanol was also tested to study the influence of copper loading on the acid-base properties of the catalysts. This approach allowed us to propose a realistic description of the copper speciation on the support surface.

2. Experimental

2.1 Synthesis of catalysts

The catalysts were prepared by the sol-gel approach by employing precursors concentration to obtain 1:1 Ti:Zr ratios and Cu loading of 1, 3 and 5 wt%. Titanium n-butoxide ($Ti(O(CH_2)_3CH_3)_4$, purity 97%, Aldrich) was mixed with ethanol in a reflux flask, and left stirring for two hours. Subsequently zirconium n-butoxide ($Zr(O(CH_2)_3CH_3)_4$, purity 76.80%, Strem Chemicals) was added, together with nitric acid (HNO_3, purity 66.3%, Reasol) to reach pH 3. The resulting solution was left under constant agitation for 24 hours before adding copper acetate ($Cu(CH_3COO)•2H_2O$, Aldrich) in the desired amount. The slurry was left stirring for 48 h, before starting the hydrolysis process by drop wise adding 20 ml of H_2O mixed with 100 ml of ethanol. The formed gels were dried at 100 ° C for 24 h and later calcined at 400 °C. The resulting CuO_x/TiO_2-ZrO_2 samples are hereafter labeled as CxTZ, where x represent the copper concentration in weight % (x = 1, 3 and 5). The TiO_2-ZrO_2 material prepared by the same way without copper is hereafter labeled as ZT.

2.2 Characterization

Gasvolumetric analysis was carried out on a Quantachrome adsorption equipment NOVA automatic (model 2002) by measuring nitrogen adsorption/desorption isotherms at liquid nitrogen temperature (LNT). Specific surface area (SSA) was calculated by the Brunauer-Emmett-Teller (BET) method.

Diffraction patterns were recorded with an X-ray diffractometer AXS D8 Bruker Advance brand, coupled to an anode copper X-ray tube (CuKα radiation) operating in the theta-theta setting at 35 kV, in the 10 to 80 ° 2θ range (step of 0.05, 1 s time per step). The measured diffractograms were compared to diffraction patterns reported in Join Commit Powder Diffraction Standard (JCPDS) cards.

Hydrogen temperature programmed reduction (H_2-TPR) experiments were carried out on a Quantachrome ChemBET TPR/TPD. A reducing gas mixture H_2/Ar (4.98% mol) was employed to heat the sample from room temperature (RT) to 700 °C in a quartz reactor with a porous bed. H_2 consumption was monitored with a thermal conductivity detector. 400 mg of C1TZ and 100 mg of C3TZ and C5TZ samples were employed for each experiment.

Diffuse Reflectance DR UV-Vis spectra were measured at RT with a Varian Cary 100 spectrophotometer (version 9) equipped with an integrating sphere of 60 mm, in the range of wavelengths from 200 to 800 nm, and a 2 nm step. $BaSO_4$ was used as a reference material. DR spectra were converted with the Kubelka-Munk function and smoothed out with 6 points Fourier filtering. Spectral deconvolution was carried out with the Gaussian fit module OriginPro8.0 software (Origin Co., USA). The maximum number of Gaussian curves to fit each spectrum was determined on the basis of the corresponding second derivative.

EPR spectra were measured at RT and LNT with a JEOL-RES3X spectrophotometer operating at the microwave frequency of 9 GHz (X-band) with a field modulated at 100 kHz and a microwave power of 1 mW. For this study, 40 mg of catalysts were placed in quartz tubes of 3 mm internal diameter. The measurements at 77 K were carried out with a quartz cryostat (Dewar Wilmar) with a fingertip. In our simulations we used the ES-PRIT JEOL software which uses analytic expressions arising from perturbation theory up to second order for the central ion and assuming Gaussian lines shapes for the EPR absorptions, as well as for the hyperfine absorptions [23]. The magnetic field was calibrated with reference to the marker diphenylpicrylhydrazyl (DPPH), which has a *g* effective value of 2.0037. The reported EPR intensities were calculated by double integration with the same JEOL ES-PRIT software. These intensities were normalized to the overall spectrum intensity of Cu^{2+} ions of C1TZ sample.

The catalytic activity of the CxTZ samples was tested in the 2-propanol decomposition reaction, as follows. 50 mg of catalysts were placed in a differential fixed bed reactor and activated at 400 °C with an argon flow of 5.4 L/h for 1.5 h. Then, 2-propanol was sent to the catalysts at 200 °C for 2 hours at atmospheric pressure by flowing Ar at 0°C through a saturator, resulting in a partial pressure of 8.28 Torr. The reaction products were analyzed by a Hewlett-Packard 5890 gas chromatograph, with a W-FFAP stainless steel column (1/8 inch of inner diameter and 2 m in length) and thermal conductivity detector.

3. Results and discussion

3.1 X-ray diffraction

The XRD patterns of the set of CxTZ samples (x = 1, 3 and 5) treated at 400 °C are reported in Fig. 1. These patterns show very poor crystallinity, in agreement with XRD results of Reddy et al. who claimed that TiO_2-ZrO_2 mixed oxides prepared by sol-gel do not crystallize at temperatures below 600 ºC [24]. A main broad peak between 20 and 40 2θ is observed, with weaker features between 40 and 70 2θ, in regions where the main diffraction peaks of monoclinic ZrO_2 are expected (JCPDS card 00-037-1484). No peaks related to cupric or cuprous oxides can be appreciated (JCPDS cards 00-048-1548 and 00-005-0667, respectively), suggesting a good dispersion of copper on the surface and in the volume (bulk) of the TiO_2-ZrO_2 matrix [25].

3.2 Gasvolumetric analysis

The results of nitrogen adsorption-desorption isotherms measured on CxTZ synthesized solids are shown in Fig. 2. All samples show a type IV isotherm (IUPAC classification) indicating that they are mesoporous [26, 27]. The hysteresis loop shape (H2 type) is commonly associated to the presence of ink-bottle shaped pores, which could be related to inter or intra-particle porosity. The SSA measured by BET method was around 244 m^2/g for all materials, including the Cu-free TZ sampler [14, 27]. The measured SSA is quite high, in agreement with X-ray diffraction studies, low crystallinity of the materials, regardless of copper content.

3.3 Temperature programmed reduction (TPR)

The TPR profiles of CxTZ samples calcined at 400 °C are reported in Fig. 3. For easier discussion the signals will be divided in two regions: between 150 and 300 °C and between 300 °C to 550 °C. Two broad and weak H_2 consumption peaks with maxima at 250 and 430 °C (labeled as T2 and T1, respectively) are observed on sample C1TZ. In both C3TZ and C5TZ samples the T1 high temperature peak is present, together with more intense and narrow components at low temperature, whose distribution changes in the two samples. More in detail, C3TZ shows in the low temperature region two intense and narrow reduction peaks, with maxima at 204 °C and 247 °C (labeled as T3 and T2, respectively), together with a component at 180 °C (T4). C5TZ sample mainly shows in the low temperature region the two intense T4 and T3 peaks at 173 and 202 °C, respectively. The described peak positions are resumed in Table 1.

The temperature maxima and integrated area of the described hydrogen consumptions curves were determined by deconvolution using Lorentzian and Gaussian functions (Table 1). The results were

also plotted as a bar diagram in Figure 4 for easier comparison. This analysis shows that the total hydrogen consumption almost triplicates passing from C1ZT to C3ZT and then slightly decreases on C5ZT. The T1 peak, with average maximum around 430 °C is present on all samples with similar intensity, suggesting that the concentration of the related reducible copper site is roughly independent on the loading. On the contrary Cu sites reduced in the low temperature region (T2, T3 and T4) are strongly dependent upon the copper loading. Namely, T2 is the dominant site in the sample with intermediate loading, while T3 slightly decreases from C3TZ to C5TZ, where the lowest reduction temperature peak T4 dominates.

All the TPR peaks described above can be related to the $Cu^{2+} \rightarrow Cu^{+}$ reduction since the TiO_2-ZrO_2 support is not expected to participate to be reduced in the employed conditions [14, 16]. Cu^{2+} ions could be present in supported CuO particles with variable size, or they could occupy structural (or interstitial) sites on the surface and in the bulk of the TiO_2-ZrO_2 matrix [28]. Each of these species is expected to give a different TPR peak whose position depends on the Cu^{2+} environment and interaction with the support.

Based on these premises, the T1 peak around 430 °C present in all samples can be assigned to isolated Cu^{2+} strongly interacting with the matrix, *e.g.* substituting for Ti^{4+} or Zr^{4+} ions in the solid solution [29, 30]. The T2 peak around 250 °C (passing from an integrated area of *ca* 18 to 63 from C1ZT to C3TZ) was assigned to the reduction of Cu^{2+} in bulk-like CuO particles supported on the TiO_2-ZrO_2 matrix [31, 32]. The lower reduction temperature (173 and 204 °C), measured for peaks T3 and T4, were instead explained with two different Cu^{2+} ions in highly dispersed supported CuO nanoparticles [33, 34]. Another interpretation found in the literature would instead propose a consecutive reduction of Cu^{2+} ions to Cu^{+} and then to Cu^{0} in supported CuO nanoparticles [35, 36]. This interpretation seems less likely in our case since one would expect to observe the T4/T3 couple with similar intensity ratio also on sample C3TZ, which is not the case.

Even though the precise assignment of the T3 and T4 peaks is not conclusive, the results point to the fact that three main Cu^{2+} sites are present in the samples: i) high reduction temperature isolated Cu^{2+} sites in the TZ solid solution, ii) supported bulk-type CuO particles with intermediate reduction temperature and iii) highly dispersed CuO supported nanoparticles/clusters with surface sites reducible at relatively low temperature. We can hypothesize that the different reducibility of T3 and T4 is related to sites on the particles surface and at the interface with the support, tuning their redox properties, or to nanoparticle and clusters with different nuclearity. Moreover, the reported TPR data clearly point to the fact that the C5TZ sample shows the more easily reduced (and thus redox active) copper sites.

3.4 DR UV-Vis Spectroscopy

The DR UV-Vis spectra of C1TZ, C3TZ and C5TZ catalysts are reported in Figure 5, together with that of TZ sample for comparison. The UV-Vis spectrum of TZ shows two maxima at 215 and 321 nm, which can be assigned to ligand to metal $O^{2-} \rightarrow Ti^{4+}$ (or Zr^{4+}) charge transfer (LMCT) transitions. This intense absorption can be also described as a transition from the valence to the conduction bands of the mixed oxide, so that the position of the absorption edge can be employed to calculate the band gap energy (E_g). This was carried out by employing the Tauc-plot method, as displayed in the Figure inset. This consists in a plot of the square of the Kubelka-Munk function *vs* the photon energy in electron-volts. The extrapolation of the linear region of the absorption edge allows calculating the E_g [37]. For TZ sample an E_g around 3.14 eV was calculated, which is similar to what usually observed for TiO_2 anatase phase. Moreover, a weak absorption tail is observed between 400 and 700 nm, which could be tentatively explained as related to defects and/or surface sites.

The UV-Vis spectra of C1TZ, C3TZ and C5TZ samples show a similar intense absorption with maxima around 217 and 295 nm, with an evident tail up to 500 nm and a broad absorption centered at 795 nm. The overall and relative intensity of the two maxima are similar in C1TZ and C5TZ samples, as compared to C3TZ, showing minor intensity and different intensity ratio. Another difference with respect to the Cu-free ZT samples is in the absorption edge position, corresponding to E_g values of 2.96, 3.09 and 2.99 eV, for C1TZ, C3TZ and C5TZ samples respectively. These features suggest an effect of copper on the electronic band structure of the TiO_2-ZrO_2 material, particularly for the C3ZT sample. More in detail the band gap energy E_g of C1ZT and C5ZT are very similar and definitely smaller with respect to the reference ZT material. On the contrary C3ZT sample shows an extrapolated edge position closer to ZT, notwithstanding sensibly different spectral shape and intensity. Thus, the increase in copper loading produces a non linear narrowing of the band gap, which can be explained with the substitution of Ti^{4+} and Zr^{4+} atoms by copper ions, as observed in Cu-doped TiO_2 synthesized by sol-gel method [38].

As for the spectral features above 400 nm (absorption tail up to 500 nm and broad band centered at 795 nm), they can be related to electronic transitions involving copper ions. Different explanations were reported in the literature for the absorption tail towards the {isible range: i) LMCT transitions in copper oxides nanoclusters [39, 40]; ii) LMCT in $(Cu\text{-}O\text{-}Cu)^{2+}$ clusters [34, 41, 42] and iii) intervalence CT transitions between Cu and Ti (or Zr) ions in the solid solution bulk [43, 44]. Noticeably a similar loading-dependent shift towards the visible region was observed in iron-doped TiO_2 samples prepared by sol-gel methods [45, 46]. Finally, the broad band centered at 795 can be ascribed to d–d transitions of

isolated Cu^{2+} ions in a distorted octahedral coordination [47, 48]. These features do not allow giving a precise speciation (type and concentration) of copper sites in the three samples. They are however in agreement with the presence of both isolated Cu^{2+} ions in the solid solution structure and CuO nanoclusters, with variable relative concentration depending on copper loading, in agreement with the TPR picture.

3.5 EPR Spectroscopy

The EPR spectra measured at 77 K on C1TZ, C3TZ and C5TZ catalysts are reported in Figure 6, together with the corresponding simulations. The spectra can be described as due to the overlapping of two main Cu^{2+} signals: one broad and asymmetric and one anisotropic with two hyperfine interactions in the $g_{\|}$ region. The former was assigned to paramagnetic Cu^{2+} ions coupled through antiferromagnetic dipolar interactions, in small oxidic clusters [41, 42]. The latter is ascribed to isolated Cu^{2+} ions in octahedral coordination with tetragonal distortion [34, 49]. The appearance of the hyperfine interaction of these Cu^{2+} ions was reported to be indicative of a high dispersion of the corresponding paramagnetic ions [50]. The two signals have an opposite trend with respect to copper loading. The anisotropic one with two hyperfine interactions decreases with copper loading increase, while the broad one dominates the spectra in the C3TZ and C5TZ samples.

EPR simulations were carried out by a linear combination method. Namely a broad axial EPR contribution (S2/S2') was added up to a signal with rhombic (S1 in sample C1ZT) or axial (S3 in samples C3TZ and C5TZ) symmetry (Figure 7). The corresponding hyperfine parameters are due to four absorption-like lines produced by coupling of the resonant spin with the magnetic moment of the copper nucleus with I = 3/2. The calculated g values for the axial ($g_{\perp}$ and $g_{\|}$) and rhombic contributions (g_{xx}, g_{yy} and g_{zz}), together with the corresponding hyperfine values (A_{xx}, A_{yy} and A_{zz}) are summarized in Table 2. In the same Table the relative and total intensity (normalized to C1TZ sample) are listed for each sample. This analysis shows that the broad axial contribution (S2/S2') accounts for 70% of the EPR signal of sample C1TZ, while the remaining part is related to the rhombic S1 site. The importance of the S2' signal increases in C3TZ and C5TZ (82 and 96% of the corresponding EPR spectra, respectively), where the remaining EPR intensity is ascribed to the axial S3 contribution.

The S2/S2' broad axial signals of the CuO_x/TiO_2-ZrO_2 series characterized by $g_{\|}$ in the range from 2.14 to 2.29 (see Table 2), can be assigned to Cu^{2+} ions in CuO clusters in which the mutual dipolar interactions between neighboring paramagnetic Cu^{2+} ions cause the widening of the EPR signals [8, 30].

As for the rhombic S1 contribution, very similar spectra were reported for octahedral Cu^{2+} ions in framework substitutional positions of copper-stabilized zirconia samples [50]. The paramagnetic axial S3 signal was instead assigned to highly dispersed Cu^{2+} ions in a tetragonally distorted octahedral symmetry [50, 51].

On this basis, the following information can be obtained. Isolated Cu^{2+} ions with octahedral symmetry are present in framework substitutional positions in all CxTZ solid solutions, but their environment is strongly dependent upon the copper loading. On the low loading C1TZ catalyst these ions are truly isolated, and they are characterized by a weakly perturbed octahedral symmetry (site S1). When copper loading increases the presence of other Cu^{2+} ions in the solid solution framework causes an axial perturbation of their symmetry, resulting in the S3 signal. On the other hand, CuO supported nanoparticles represent the majority of copper species in all samples. The amount of this kind of interacting resonant ions reaches a maximum at intermediate loading (sample C3TZ). This is not surprising since further agglomeration at higher loading causes a strong interaction between Cu^{2+} ions which suppress the EPR signal [52].

4. Catalytic activity

The decomposition of 2-propanol was employed as a test reaction to get information on the acid-base properties of CxTZ materials, in that the selectivity to propene or to acetone implies the presence of acid or basic sites, respectively [27]. The results are summarized in Table 3, together with the measured reaction rate. This parameter is strongly influenced by the copper content, suggesting that this metal has a major role on the catalytic activity in the 2-propanol decomposition. On the Cu-free TiO_2-ZrO_2 catalyst the major product is propene, in agreement with the strong acidic properties of the cations at the surface of the mixed oxide [27]. The selectivity pattern is greatly affected by copper, with a strong dependence upon its amount, so that acetone is the main product (88%) formed on catalyst C5TZ. This suggests an increase in the basic properties of the catalysts related to the copper species highly dispersed on the support surface [53]. This reactivity is prevailing on that related to propene formation through acid sites, which could be still present on the TiO_2-ZrO_2 support or could be related to the amphoteric nature of the supported CuO [54].

Discussion

The nature of copper sites in CuO_x/TiO_2-ZrO_2 samples prepared by sol-gel method was studied by different characterization techniques. TPR results point to the presence of four Cu^{2+} ions with different

redox behaviuor (Figure 8). T1 sites, interpreted as substitutional framework ions in the TZ solid solutions, are isolated Cu^{2+} ions with high reduction temperature. These sites are present in all samples, with different concentration, and are responsible for the observed shift of the TiO_2-ZrO_2 edge position and for the d-d absorption band at 800 nm in the UV-Vis spectra of the catalysts. There is not a linear correlation between copper loading and edge position, suggesting that complex phenomena can occur in the one-pot sol-gel process hen copper is added to the mixture.

The framework isolated Cu^{2+} sites give a rhombic EPR signal (S1) in the low loading C1TZ sample, indicating a weakly perturbed octahedral symmetry. When the copper loading increases, even if the Cu^{2+} ions are still isolated as concerning their first coordination shell, their local symmetry is perturbed by the presence of other substitutional Cu^{2+} ions in close positions. Their octahedral symmetry is further perturbed, resulting in an axial EPR signal (S3), so that they can be defined as "quasi-isolated" sites. Due to the high reduction temperature, these sites are likely to show a negligible catalytic activity.

Two different kind of CuO supported nanoparticles were observed by TPR experiments. The so-called "bulk-like" type, mainly present in sample C3TZ, showed a relatively high reduction temperature (T2). On the contrary, highly dispersed CuO nanoparticles could be detected in all samples, and their presence is particularly relevant on sample C5TZ. The Cu^{2+} ions in these particles give two defined TPR peaks at low temperature (T3 at 202-204 and T4 at 173 °C), which could be related to sites on the surface of nanoparticles and at the interface with the TiO_2-ZrO_2 support or to the presence of nanoparticles/clusters with different nuclearity. The low temperature reduction peak (T4) is particularly important in sample C5TZ. Again, the not linear correlation with copper loading can be related to the influence of copper addition in the sol-gel mixture.

The CuO nanoparticles/clusters are responsible for the low frequency tail of the DR UV-Vis TiO_2-ZrO_2 absorption edge up to 550 nm observed in all samples. This spectral feature is particularly evident in the highest loading C5TZ sample, suggesting a high amount of clustered oxidic species. Accordingly, EPR spectra showed a broad axial signal (S2/S2') in all samples, assigned to interacting Cu^{2+} ions in CuO clusters. The intensity of this EPR contribution is dominant in all samples, in good agreement with TPR results. Moreover, it reaches a maximum on sample C3TZ, indicating further agglomeration (suppressing EPR signal) in the high loading C5TZ sample.

Conclusions

Three CuO_x/TiO_2-ZrO_2 catalysts with different copper loading (1, 3 and 5 wt%) were prepared by one-step sol-gel method and calcined at relatively low temperature (400 °C). This procedure resulted

in high surface area materials (specific surface area around 250 m^2/g, irrespective of the copper content) with small particle size and poor crystallinity, as determined by PXRD. The catalysts were characterized with particular attention to the nature and properties of the copper species by three main techniques, namely hydrogen TPR, DR UV-Vis and EPR techniques. All techniques point to the presence of different copper species, with a loading dependent distribution.

More in detail, TPR suggested the presence of 4 different reducible Cu^{2+} ions, with different concentration on the three samples (Figure 8). One high temperature reduction site (T1) was assigned to Cu^{2+} ions in the solid solution bulk. This site was present on all samples with comparable concentration, slightly decreasing with copper loading increase. More easily reducible Cu^{2+} sites (T2, peak at 250°C) were assigned to bulk-like CuO particles. It is noteworthy that no CuO peaks could be observed by XRD, thus suggesting that these particles are relatively small and supported on the TiO_2-ZrO_2 support. Two other Cu^{2+} sites were reduced at around 170 and 200 °C (T4 and T3, respectively), suggesting the presence of highly dispersed nanosized CuOx particles or clusters.

The picture coming from TPR analysis was in agreement with DR UV-Vis measurements. These results showed a modification of the TiO_2-ZrO_2 mixed oxide band gap with copper introduction, suggesting its insertion in bulk positions. This was also confirmed by the presence of a band around 800 nm related to d-d transitions of octahedral Cu^{2+} ions. Another important feature, strongly dependent upon copper loading, was a broad absorption tail below 400 nm, easily assigned to LMCT transitions in CuO particles of different size and nuclearity.

EPR measurements showed two main signals: one broad and asymmetric and one anisotropic with two hyperfine interactions in the g|| region. The former was assigned to paramagnetic Cu^{2+} ions coupled through antiferromagnetic dipolar interactions in small oxidic clusters, while the latter could be explained by the presence of Cu^{2+} ions in distorted octahedral coordination. Spectra simulation allowed to discriminate among 4 different contributions (S1, S2/S2' and S3) and to calculate their concentration in the different samples. The picture rising from this analysis confirmed the presence of Cu^{2+} ions in the solid solution bulk, in agreement with TPR and UV-Vis. Moreover, it was shown that the local environment of these ions was affected by copper loading, in that the symmetry changed from rhombic in the low loading sample (S1, isolated sites) to axial (S3, quasi-isolated sites) at increasing loading. The broad and asymmetric signal, with g|| in the range from 2.14 to 2.29 (S2 and S2') was assigned to Cu^{2+} ions interacting in small CuOx clusters or nanoparticles. These species are likely to be the ones with TPR peaks at 170 and 200 °C (T4 and T3). This assignment was confirmed by the decrease of the EPR signals

intensity in the higher copper loading sample (5 wt %), where larger agglomeration (suppressing the EPR signals due to strong interaction between Cu^{2+} ions) was suggested by DR UV-Vis measurements.

Finally, the surface acidity and basicity of the mixed oxides was characterized by analyzing reaction rate and selectivity pattern of the 2-propanol decomposition. These data were compared to those measured on Cu-free TiO_2-ZrO_2 mixed oxide, whose main product was propene (53%), in agreement with the well-known strong acidity of both Zr^{4+} and Ti^{4+} ions. Both reaction rates and selectivity to acetone were strongly affected by copper loading, suggesting the important role of the corresponding species (mainly CuOx clusters or particles of different nuclearity and reducibility) on the surface chemistry of the materials.

Acknowledgements

To the projects: PROMEP-Mexico and COFAA-IPN for support. F. Chavez-Rivas acknowledge technical support from Dr. Rafael Zamorano Ulloa from ESFM-IPN and Dr. Sakhno Yuri and Dr. Marco Fabbiani of the Department of Chemistry and NIS center of the University of Turin, Italy. Authors would like to acknowledge to Dr. Raúl Pérez Hernández for fruitful discussions.

Tables

Table 1 TPR position and intensity calculated for the CxTZ series and corresponding assignment

Sample	Peak labels	Peak maximum (°C)	Integrated area (a. u.)	Assignment
C1TZ	T1	430	6.8	Cu^{2+} in solid solution
	T2	250	18.2	CuO bulk-like
C3TZ	T1	445	21.9	Cu^{2+} in solid solution
	T2	247	63.2	CuO bulk-like
	T3	204	46.9	Nano CuO highly dispersed
	T4	180	11.9	Cu^{2+} on support surface
C5TZ	T1	425	20.5	Cu^{2+} in solid solution
	T3	202	44.7	Nano CuO highly dispersed
	T4	173	54.0	Cu^{2+} on support surface

Table 2 Spin-Hamiltonian parameters of Cu^{2+} centers in the CxTZ series, obtained from computer simulation of the EPR spectra reported in Figure 6.

[a]

Sample	Site	$g_{xx}(g_{\perp})$ [a]	g_{yy} [a]	$g_{zz}(g_{II})$ [a]	$A_{xx}(A_{\perp})$ [b] (mT)	A_{yy} [b] (mT)	$A_{zz}(A_{II})$ [b] (mT)	Relative Intensity[c]	Total Intensity[c]
C1TZ	S1	2.09	2.06	2.34	2.0	0	13.0	0.30	1
	S2	2.10	2.10	2.14	0	0	0	0.70	
C3TZ	S3	2.07	2.07	2.37	0	0	13.5	0.27	1.5
	S2’	2.13	2.13	2.29	0	0	0	1.23	
C5TZ	S3	2.07	2.07	2.38	0	0	13.5	0.05	1.3
	S2’	2.13	2.13	2.29	0	0	0	1.25	

Estimated error ±0.01. [b] Estimated error ±0.2. [c] Intensities normalized to the intensity of C1TZ sample.

Table 3 Catalytic activity of the CxTZ catalysts in the decomposition of 2-propanol: selectivity and reaction rate.

Catalyst	Selectivity %			v_r	Reference
	Propene	Acetone	Isopropyl ether	(mol/s g_{cat} x 10^7)	
TZ	53	26	22	0.3	[27]
C1TZ	68	32		3.7	this work
C3TZ	55	45		5.0	this work
C5TZ	12	88		12.0	this work

References

[1] Y.J. Li ,W.K. Hall, J. Phys. Chem., 94 (1990) 6145-6148.
[2] M. Shelef, Chem. Rev., 95 (1995) 209-225.
[3] B. Guan, R. Zhan, H. Lin ,Z. Huang, Appl. Therm. Eng., 66 (2014) 395-414.
[4] S. Andonova, E. Vovk, J. Sjoblom, E. Ozensoy ,L. Olsson, Appl. Catal. B-Environ., 147 (2014) 251-263.
[5] F. Giordanino, E. Borfecchia, K.A. Lomachenko, A. Lazzarini, G. Agostini, E. Gallo, A.V. Soldatov, P. Beato, S. Bordiga ,C. Lamberti, J. Phys. Chem. Lett., 5 (2014) 1552-1559.
[6] C. Lamberti, S. Bordiga, M. Salvalaggio, G. Spoto, A. Zecchina, F. Geobaldo, G. Vlaic ,M. Bellatreccia, J. Phys. Chem. B, 101 (1997) 344-360.
[7] V.Z. Fridman ,A.A. Davydov, J. Catal., 195 (2000) 20-30.
[8] A. Martínez-Arias, M. Fernández-García, et al., J. Catal., 195 (2000) 207-206.
[9] Y. Gong, H. Chen, Y. Chen, X. Cui, Y. Zhu, X. Zhou ,J. Shi, Microporous Mesoporous Mater., 173 (2013) 112–120.
[10] D.S. Brands, E.K. Poels ,A. Bliek, Appl. Catal. A-Gen., 184 (1999) 279-289.
[11] A. Adamski, Z. Sojka, K. Dyrek, M. Che, G. Wendt ,S. Albrecht, Langmuir, 15 (1999) 5733-5741.
[12] S. Wang, D. Mao, X. Guo, G. Wu ,G. Lu, Catal. Commun., 10 (2009) 1367-1370.
[13] J. Oi-Uchisawa, S.Wang, T.Nanba, A. Ohi ,A. Obuchi, Appl. Catal. B-Environ., 44 (2003) 207–215.
[14] V. Idakiev, T. Tabakova, K. Tenchev, Z.Y. Yuan, T.Z. Ren, A. Vantomme ,B.L. Su, J. Mater. Scie., 44 (2009) 6637-6643.
[15] M. Haneda, Kintaichi, M. Inaba ,H. Hamada, Catal. Today, 1998 (1998) 127–135.
[16] Y. Kintaichi, M. Haneda, M. Inaba ,H. Hamada, Catal. Lett., 48 (1997) 121-127.
[17] M. Tajima, M. Niwa, Y. Fujii, Y. Koinuma, R. Aizawa, S. Kushiyama, S. Kobayashi, M. Mizuno ,H.O. Chi, Appl. Catal. B-Environ., 14 (1997) 97–103.
[18] B.M. Reddy ,A. Khan, Catal. Rev.-Sci. Eng., 47 (2005) 257–296.
[19] A.E. McHale ,R.S. Roth, J. Am. Ceram. Soc., 69 (1986) 827-832.
[20] A. Baiker, P. Dollenmeier, M. Glinski ,A. Reller, Appl. Catal., 35 (1987) 365-380.
[21] J.A. Navio, M. Macias ,P.J. Sanchez-Soto, J. Mater. Sci. Lett., 11 (1992) 1570-1572.
[22] I.C. Cosentino, E.N.S. Muccillo, R. Muccillo ,F.M. Vichi, J. Sol-Gel Sci. Technol., 37 (2006) 31–37.
[23] Manual JEOL, ES-PRIT Series, ESR data system (System version 1.6), [4] Simulation, No. IER-PRIT-SIM-1 (ER630001-/631001-1, 1991).
[24] C.B. Reddy B. M, Ganesh I, Reddy E. P, Rojas T. C, and Fernández A., J. Phys. Chem. B. , 102 (1998) 10176-10182.
[25] B.M. Reddy, M. B ,R.E. P, Langmuir, 9 (1993) 1781-1785.
[26] P. Harrison, I. K. Ball, W. Azelee, W. Daniell and D. Goldfarb, Chem. Mater., 12 (2000) 3715-3725.
[27] M.E. Manríquez, T. López, R. Gómez and J. Navarrete, J. Mol. Catal. A -Chem., 220 (2004) 229–237.
[28] E. Moretti, L. Storaro, A. Talon, P. Patrono, F. Pinzari, T. Montanari, G. Ramis ,M. Lenarda, Appl. Catal. A-Gen., 344 (2008) 165–174.
[29] F. Amano, S. Suzuki, T. Yamamoto ,T. Tanaka., Appl. Catal. B-Environ., 64 (2006) 282–289.
[30] G.V. Sagar, P. Rao, C. Srikanth ,K. Chary, J. Phys. Chem. B, 110 (2006) 13881-13888.
[31] C. Yao, L.C. Wang, Y.M. Liu, G.S. Wu, Y. Cao, W.L. Dai, H.Y. H ,K.N. Fan, Appl. Catal., A: General 297 (2006) 151-158.
[32] J. Słoczynski, R. Grabowski, A. Kozłowska, P.K. Olszewski ,J. Stoch, Phys. Chem. Chem. Phys., 5 (2003) 4631–4640.

[33] T.-J. Huang, Kuen-Cheung Lee, Hsiao-Wen Yang, Wei-Ping Dow, Appl. Catal. A-Gen., 174 (1998) 199-206.
[34] K.V.R. Chary, G.V. Sagar, D. Naresh, K.K. Seela ,B. Sridhar, J. Phys. Chem. B, 109 (2005) 9437-9444.
[35] G.-H. Lee, M.S. Lee, G.-D. Lee, Y.-H. Klm ,S.-S. Hong, J. Ind. Eng. Chem., 8 (2002) 572-577.
[36] L. Xiaowei, Shen Mingmin, Hong Xi, Zhu Haiyang, Gao Fei, Kong Yan. Dong Lin, and Chen Yi, J. Phys. Chem. B, 109 (2005) 3949-3955.
[37] D. Wood ,J. Tauc, Phys. Rev. B, 5 (1972) 3144- 3151.
[38] R. Lopez, R. Gomez ,M.E. Llanos, Catal. Today, 148 (2009) 103–108.
[39] H. Irie, S. Miura, K. Kamiya ,K. Hashimoto, Chem. Phys. Lett., 457 (2008) 202–205.
[40] X. Qiu, M. Miyauchi, K. Sunada, M. Minoshima, M. Liu, Y. Lu, D. Li, Y. Shimodaira, Y. Hosogi, Y. Kuroda ,K. Hashimoto, ACS Nano, 6 (2012) 1609–1618.
[41] Z. Liu, M.D. Amiridis ,Y. Chen, J. Phys. Chem. B, 109 (2005) 1251-1255.
[42] L. Dong, Lianjun Liu, Yuanyuan Lv, Jie Zhu, Haiqin Wan, Bin Liu, Fei Gao, Xiaoshu Wang, J. Mol. Catal. A -Chem., 365 (2012) 87– 94.
[43] C. Ampelli, R. Passalacqua, C. Genovese, S. Perathoner, G. Centi, T. Montini, V. Gombac, J.J.D. Jaen ,P. Fornasiero, RSC Adv., 3 (2013) 21776–21788.
[44] B. Choudhury, M. Dey ,A. Choudhury, Int. Nano Lett., 3:25 (2013) 8.
[45] L. Wen ,X.Z. B. Liu, Kazuya Nakata, Taketoshi Murakami, and Akira Fujishima, Int. J. Photoenergy, 2012 (2012) 10.
[46] L.Y. Zhu, X.T. Liu, W.W. Qin, X.S. Liu, N.N. Cai, X.Q. Wang, X.J. Lin, G.H. Zhang ,D. Xu, Mater. Res. Bull., 48 (2013) 2737–2745.
[47] V. Indovina, M. Occhiuzzi, D. Pietrogiacomi, and S. Tuti, J. Phys. Chem. B, 103 (1999) 9967-9977.
[48] O.V. Komova, S. A.V., R. V.A., K.D. I., O. G.V., K. V.V. ,P. E.A., J. Mol. Catal. A -Chem., 161 (2000) 191–204.
[49] H. Zhu, Dong L, Chen Y., J. Colloid Interface Sci., 357 (2011) 497-503.
[50] V. Ramaswamy, M. Bhagwat, D. Srinivas ,A.V. Ramaswamy, Catal. Today, 97 (2004) 63-70.
[51] F. Amano, S. Suzuki, T. Yamamoto ,T. Tanaka, Appl. Catal. B-Environ., 64 (2006) 282–289.
[52] F. Mehran, S.E. Barnes, G.V. Chandrashekhar, T.R. Mc Guire ,M.W. Shafer, Solid State Commun., 67 (1988) 1187-1189
[53] J.I. Di Cosimo, G. Torres, C.R. Apesteguía, J. Catal., 208 (2002) 114–123.
[54] K. Dyrek, Michel Che, Chem. Rev., 97 (1997) 305-331.

Figure captions

Figure 1 X-ray diffraction patterns of the CxTZ (x = 1, 3, 5) catalysts calcined at 400 °C.

Figure 2 Gasvolumetric nitrogen adsorption/desorption isotherms measured on CxTZ (x = 1, 3, 5) catalysts.

Figure 3 TPR profiles of a) C1TZ, b) C3TZ and c) C5TZ.

Figure 4 Bar plot of the integrated areas of H_2 consumption peaks measured on CxTZ (x = 1, 3, 5) catalysts.

Figure 5 DR UV-Vis spectra of TiO_2-ZrO_2 (full line), C1TZ (dashed-dotted), C3TZ (dashed) and C5TZ (dotted). The inset reported the corresponding Tauc plot.

Figure 6 EPR spectra measured at 77 K of C1TZ, and C5TZ C3TZ catalysts, with corresponding simulations (see text for details).

Fig. 7 EPR components employed to simulate the experimental spectra.

Fig. 8 Pictorial representation of copper species observed on the CuO_x/TiO_2-ZrO_2 catalysts studied in this work. T and S labels refer to the assignments proposed in TPR and EPR sections (Tables 1 and 2).

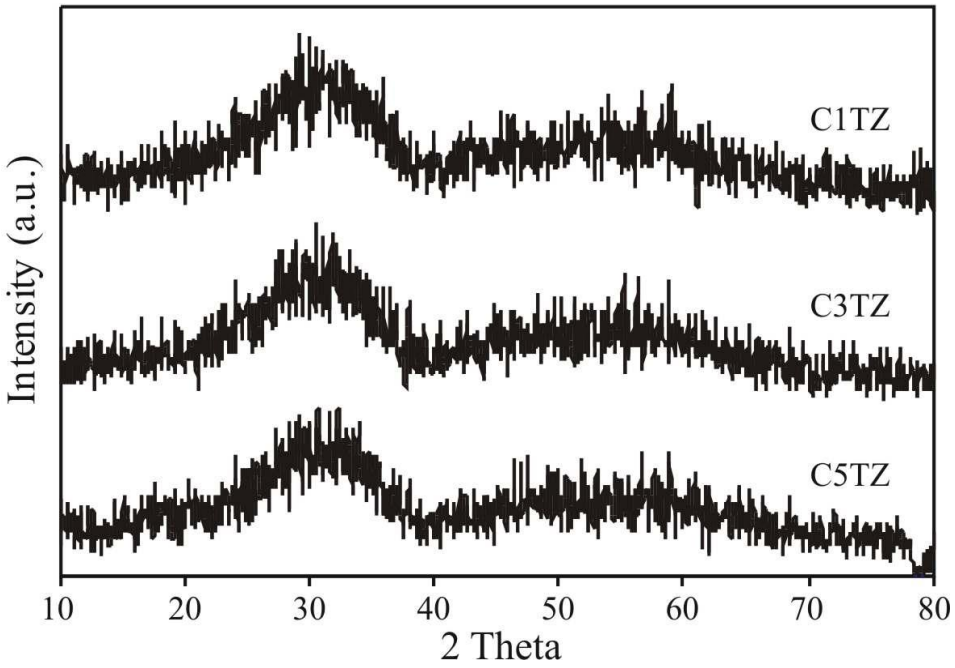

Figure 1

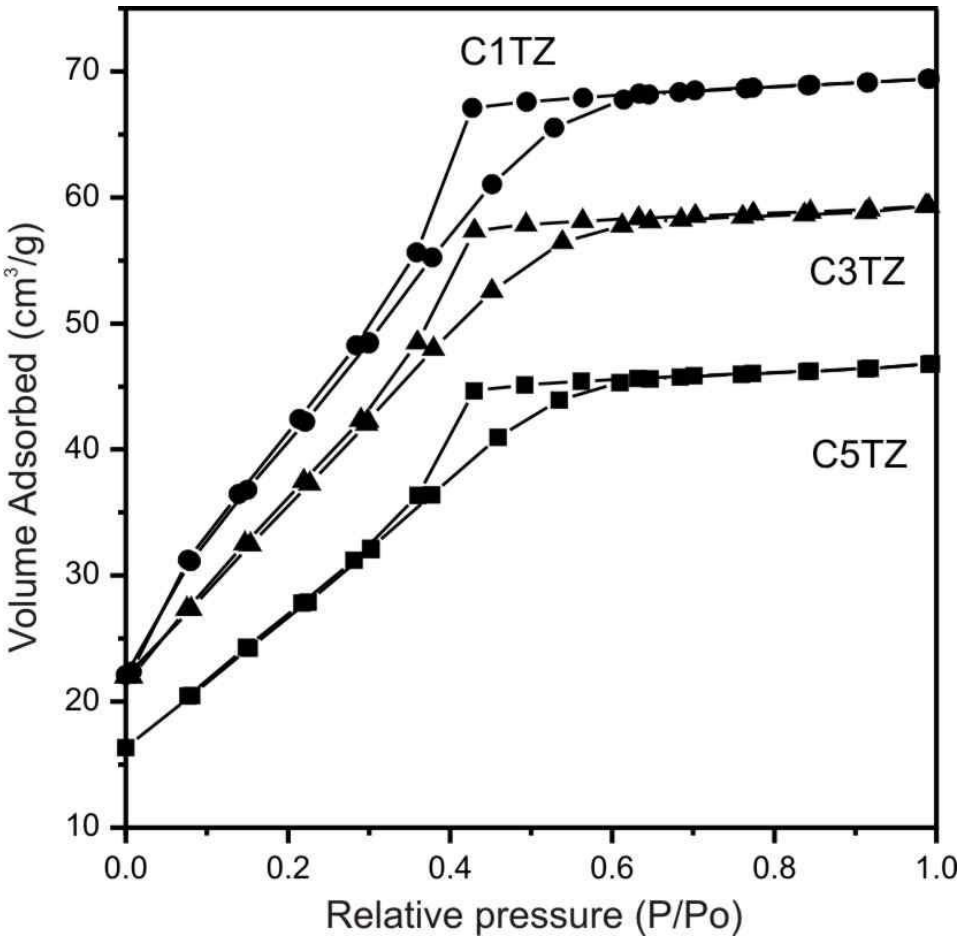
C1TZ
C3TZ
C5TZ
Volume Adsorbed (cm3/g)
Relative pressure (P/Po)
70
60
50
40
30
20
10
0.0
0.2
0.4
0.6
0.8
1.0
Figure 2

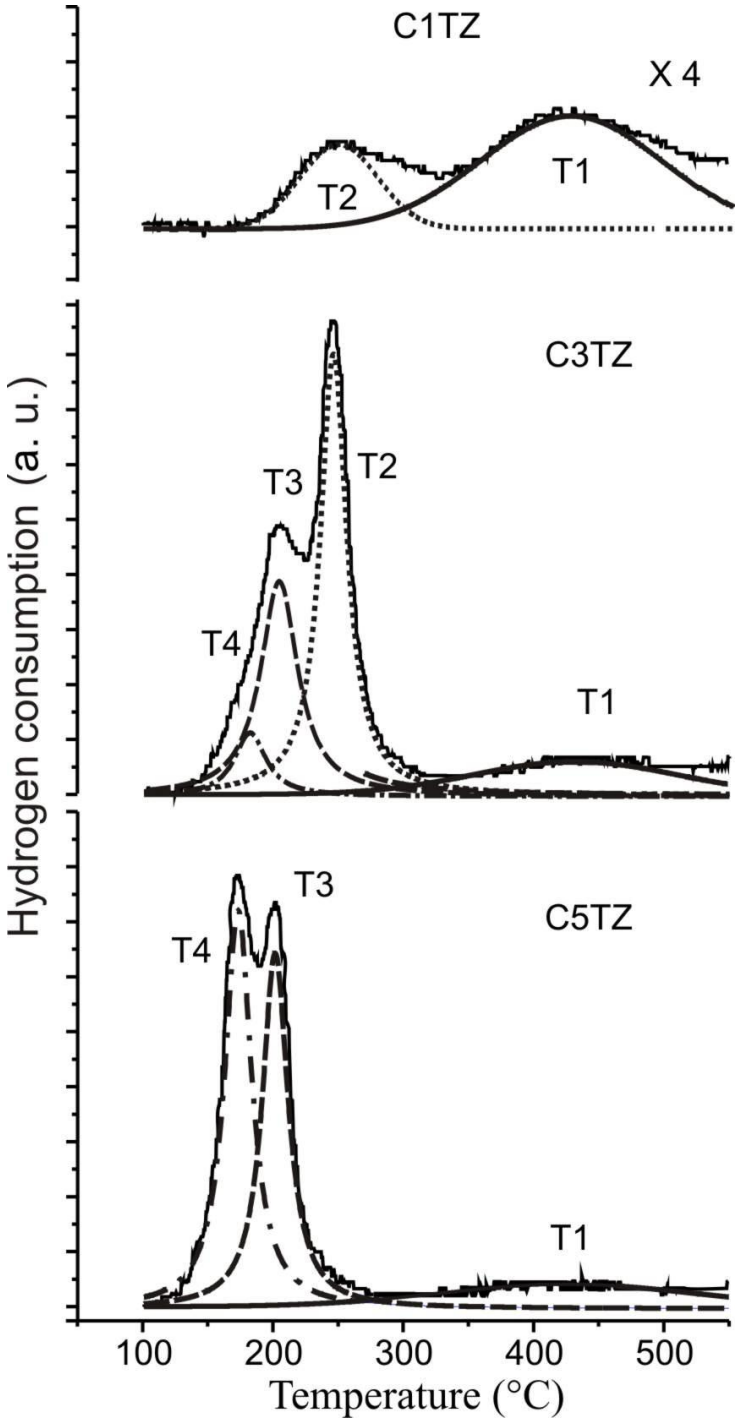
C1TZ
X 4
T2
T1
C3TZ
T3
T2
T4
T1
C5TZ
T3
T4
T1
Hydrogen consumption (a. u.)
100
200
300
400
500
Temperature (°C)

Figure 3

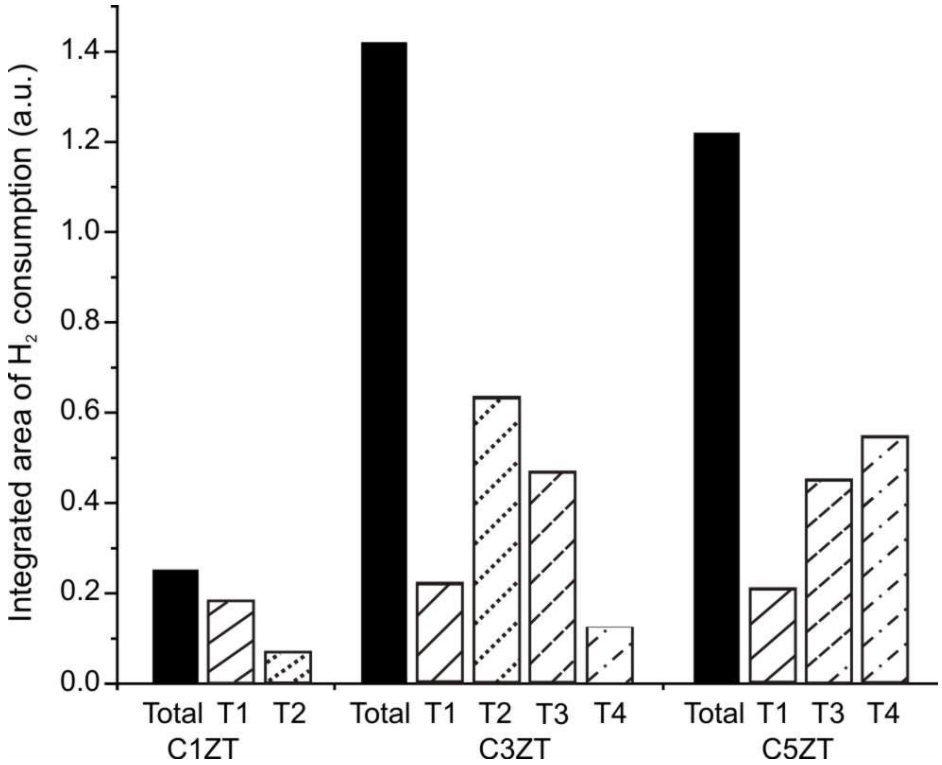
Integrated area of H_2 consumption (a.u.)
1.4
1.2
1.0
0.8
0.6
0.4
0.2
0.0
Total T1 T2
C1ZT
Total T1 T2 T3 T4
C3ZT
Total T1 T3 T4
C5ZT
Figure 4

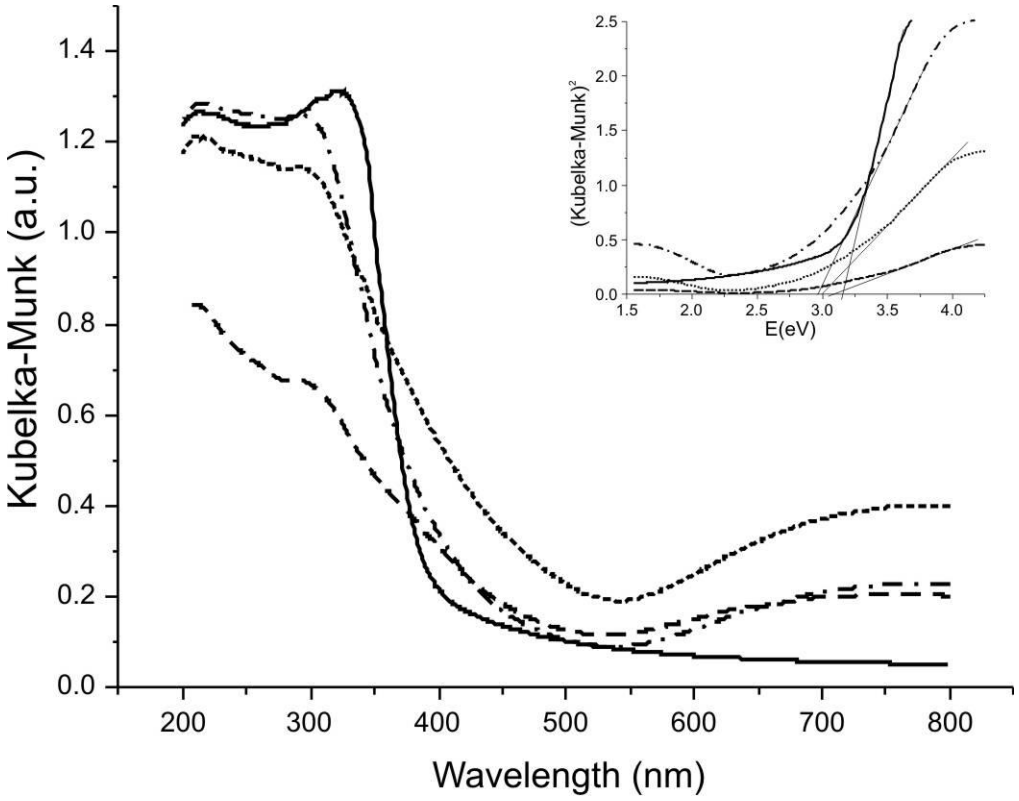

Figure 5

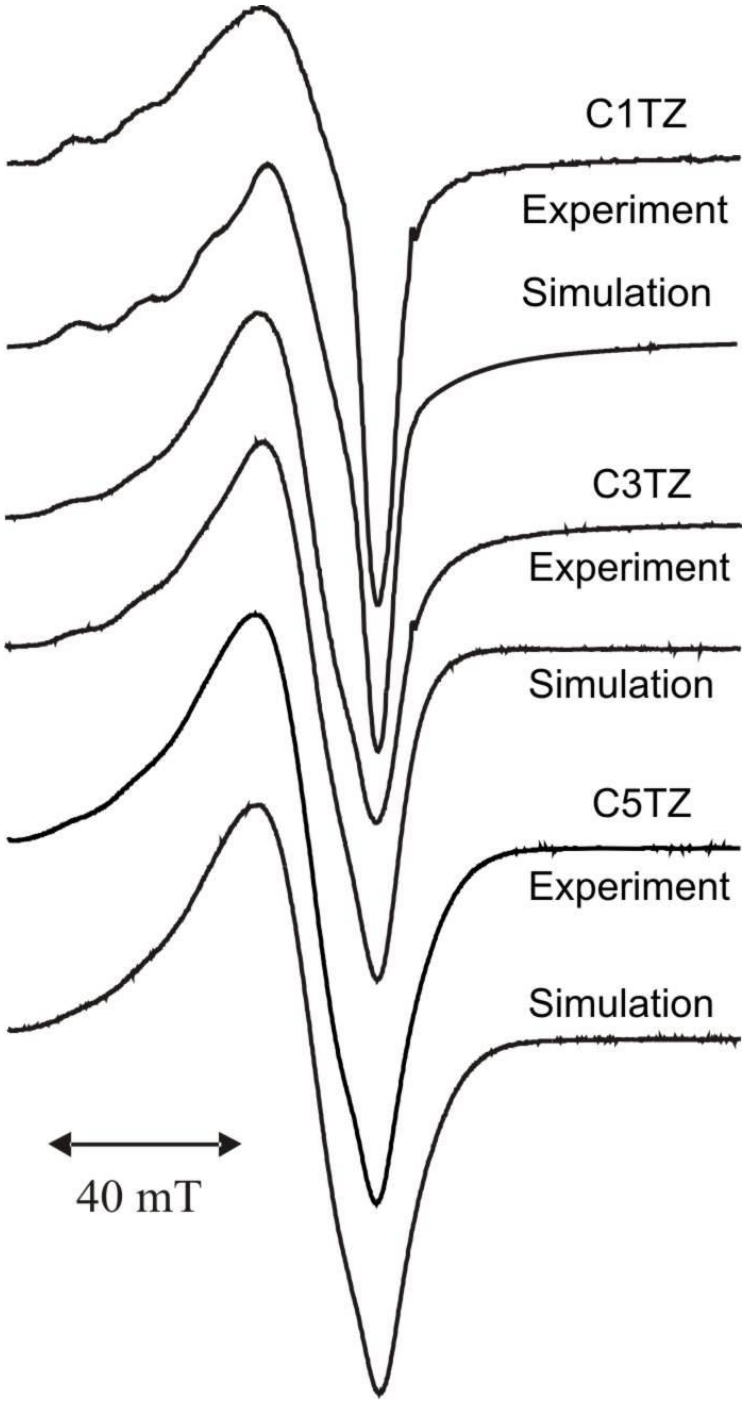
C1TZ
Experiment
Simulation
C3TZ
Experiment
Simulation
C5TZ
Experiment
Simulation
40 mT

Figure 6

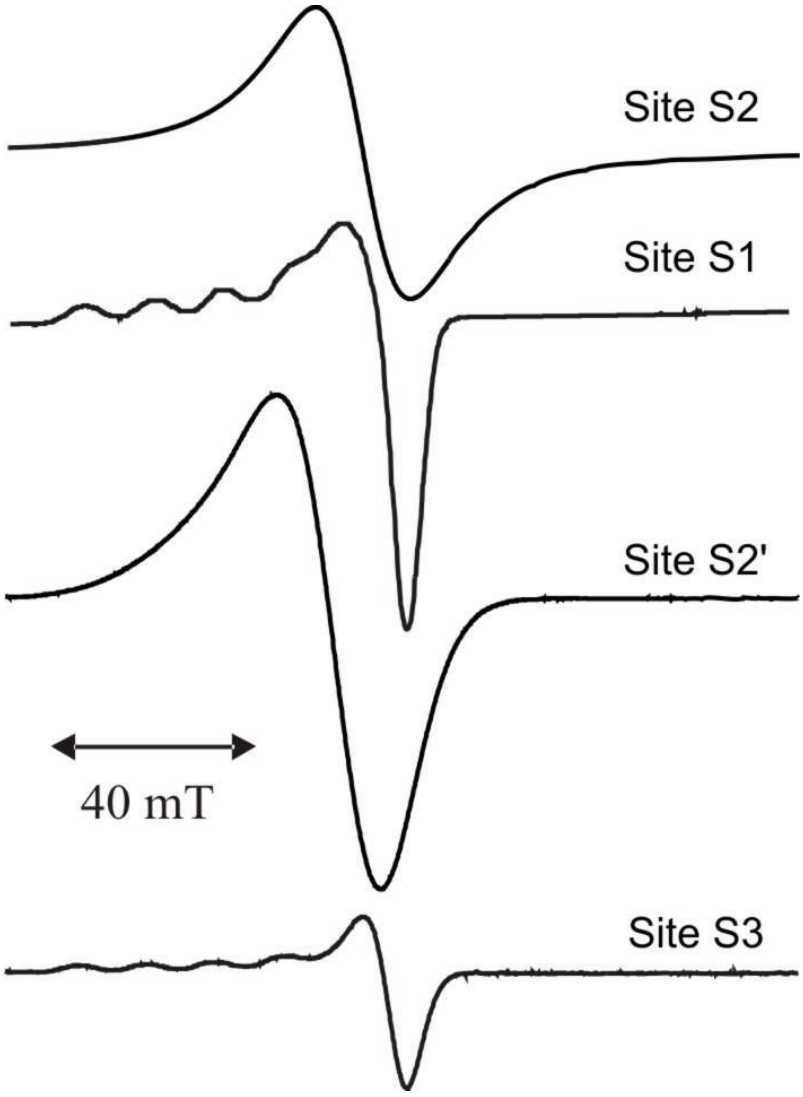

Figure 7

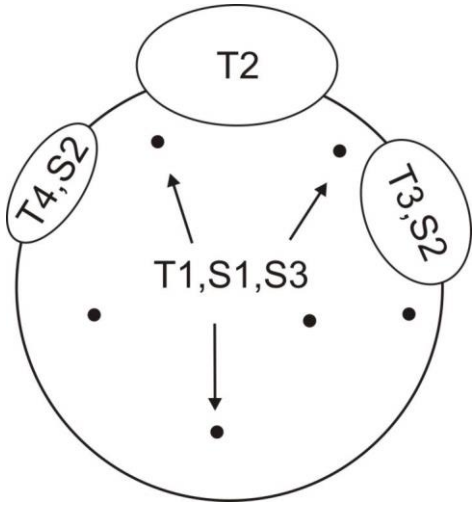

Figure 8

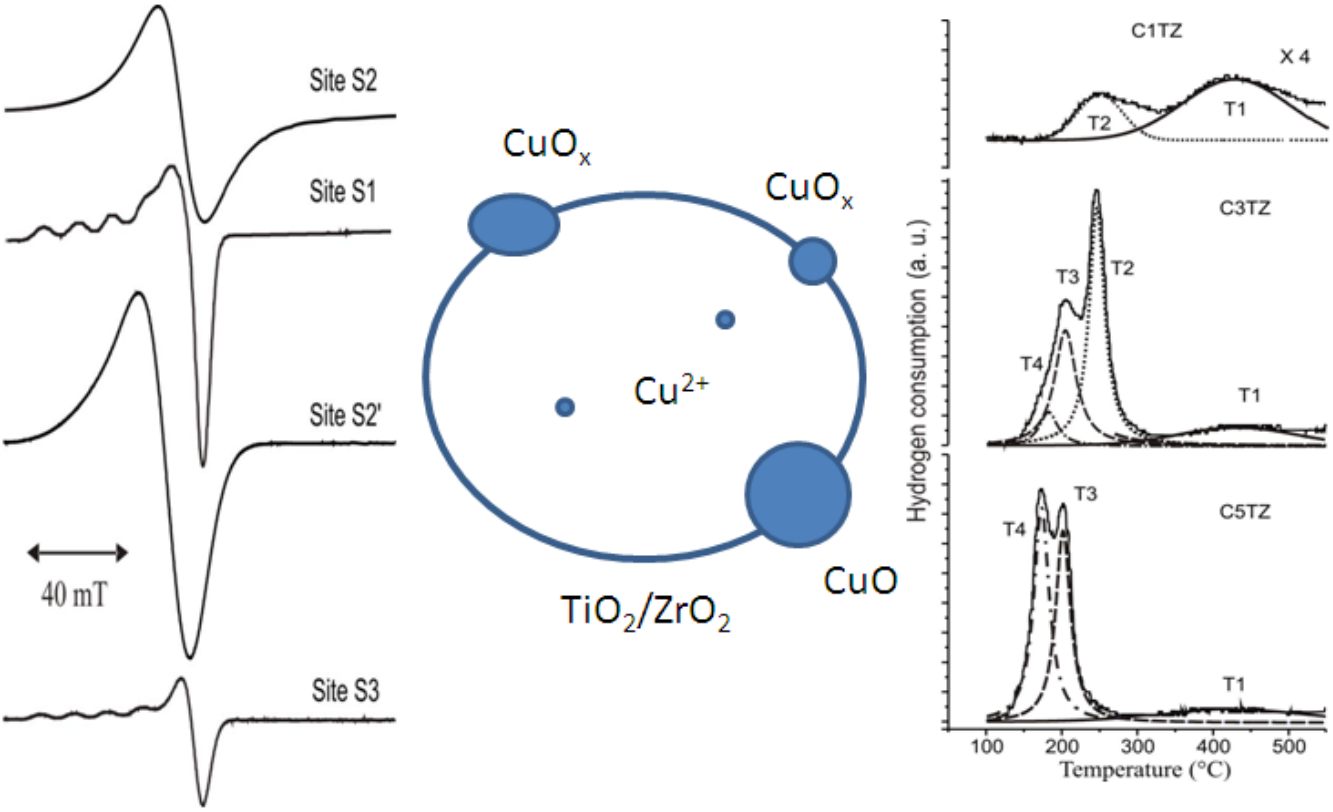

Graphical abstract